



Sharif University of Technology
Scientia Iranica
Transactions B: Mechanical Engineering
<http://scientiairanica.sharif.edu>



Magneto-hydrodynamic mixed convective heat transfer in a nanofluid filled wavy conduit with rotating cylinders

M. Mokaddes Ali^{a,*}, S. Rushd^b, R. Akhter^c, and M.A. Alim^d

a. *Department of Mathematics, Mawlana Bhashani Science and Technology University, Tangail 1902, Bangladesh.*

b. *Department of Chemical Engineering, King Faisal University, Al Ahsa, Saudi Arabia.*

c. *Department of Electrical and Electronic Engineering, The International University of Scholars, Dhaka 1212, Bangladesh.*

d. *Department of Mathematics, Bangladesh University of Engineering and Technology, Dhaka 1000, Bangladesh.*

Received 16 July 2020; received in revised form 25 May 2021; accepted 4 October 2021

KEYWORDS

Mixed convection;
 Nanofluids;
 Inclined magnetic field;
 Rotating cylinders;
 Finite element method;
 Wavy conduit.

Abstract. Flow and thermal characteristics of mixed convection in a nanofluid filled wavy conduit were numerically investigated in this study. The conduit was considered to contain a pair of rotating cylinders. It was heated and cooled from its lower and upper wavy surfaces, respectively. The rotating cylinders were placed along the centerline of the wavy conduit. It was also permeated by an external magnetic field. Finite element method was employed to simulate the conservation equations. Based on the current investigation, a new model was developed to improve the thermal conductivity of nanofluids inside a wavy conduit. In addition, a detailed parametric study was conducted to visualize the effects of dimensionless key parameters on the flow structure and temperature field in the conduit. The numerical results indicated that the physical parameters could noticeably affect both fluid flow using streamlines and temperature distributions using isotherm contours and average Nusselt number. The rotating cylinders, wavy surfaces, and inclined magnetic field were found to have the most significant effects on the heat transfer mechanism. Maximum heat transfer occurred when placing the magnetic field at an angle of 90° .

© 2022 Sharif University of Technology. All rights reserved.

1. Introduction

Dedicated research on the mixed convection in a closed or open enclosure is essential due to its industrial and engineering applications such as heat exchangers, electronic cooling, nuclear reactors, solar technologies, and air conditioning. Examination of the performance

of different cooling systems is a major challenge in thermal engineering. Several numerical and experimental studies have been performed to enhance the efficiency of different thermal equipment based on different mechanisms such as improving design, using novel fluids for heat transfer, and developing new mathematical models to name a few. In addition, the effect of magnetic field on natural or mixed convection has drawn considerable attention due to its important role in controlling convective flow as well as thermal behaviors in engineering. Some of the most significant studies in these fields are discussed below.

A finite element solution for lid-driven mixed convection in a square cavity demonstrated the occurrence of less heat transfer near the wall in case

*. *Corresponding author. Tel.: +88 01743939681; Fax: +88 0921 51900*
E-mail addresses: mmali309@gmail.com (M. Mokaddes Ali); mrushd@ualberta.ca (S. Rushd); dr.rousanara@ius.edu.bd (R. Akhter); maalim@math.buet.ac.bd (M.A. Alim)

of uniform heating, and vice versa [1]. The local average Nusselt number as well as the transition of flow pattern in forced convection from free convection caused by Reynolds number depended on Grashof number. Later on, the finite volume technique was employed to investigate the mixed convection in a cavity with top wall motion and a corner heater [2]. The heat transfer rate was recorded as a decreasing function of Hartman number, which became prominent at larger Grashof number. Another finite volume analysis of mixed convection in a vertical lid-driven square enclosure exhibited the increasing magnitude of the magnetic field strength to increase the drag coefficient and decrease the heat transfer rate [3]. Another numerical study was conducted to examine the impact of magnetic field on the natural convection in a trapezoidal enclosure [4] according to which higher values of magnetic strength and wall inclination angle reduced the heat transfer rate. Sivasankaran et al. [5] employed finite volume method to conduct a numerical analysis of mixed convection in a lid-driven cavity whose vertical walls were partially heated in the presence of magnetic field effect. In their study, two similar and dissimilar locations of heating and cooling walls were considered. They found that in the case of similar locations of partially thermally active walls, the average heat transfer rate increased compared to the case of dissimilar locations. Therefore, the existing numerical results of the convective fluid flow and temperature fields in different geometries with dissimilar thermal conditions in the presence of magnetic field substantiated the limitations of lower thermal conductivity in a traditional heat transfer fluid that impeded the improvement of heat transfer efficiency in modern technologies.

Taking into account the industrial demands for higher cooling efficiency, Maxwell [6] developed a thermal conductivity model based on the amalgamation of millimeter- or micrometer-sized particles into the traditional fluids. However, the practical implementation of this research outcome faced some notable limitations including rapid sedimentation, erosion, clogging, and high-pressure drop. A new technology has been developed in recent years to overcome these limitations using nanofluids, which are colloidal mixtures of nanometer-sized particles (metal or metal-oxide) and traditional heat transfer fluids. This type of heat transfer fluids originates from the Argonne National Laboratory [7]. Stability and higher thermal conductivity of these novel fluids make them suitable for practical applications in heat transfer processes. Several numerical studies have been conducted to date in this regard. A selected number of pertinent research outcomes available in the literature are discussed in the following.

Fereidoon et al. [8] employed a finite volume technique to analyze mixed convection flow in an

Al_2O_3 /water nanofluid filled inclined square cavity with two moving walls. They noted that the heat transfer rate differed from Richardson number and Reynolds number due to solid volume fraction of nanoparticles. This analysis was extended later to an inclined magnetic field in the presence of discrete heater to identify the entropy generation and average Nusselt number as sensitive to a number of selected parameters [9]. Through a numerical investigation of the mixed convection flow of nanofluid in an inclined trapezoidal cavity with a lid-driven wall, Kareem et al. [10] found the average Nusselt number to be directly influenced by not only different concentrations and diameters of the nanoparticles, but also inclination angle and aspect ratio. They also noted that the heat transfer rate would be greater in aiding flow than that in opposing flow. M'hamed et al. [11] presented a brief review to better understand the effect of the external magnetic field on nanofluids particles and flow as well. These investigations explored the fluid flow and heat transfer enhancement simple configurations under different boundary conditions, considering nanofluids in the presence of magnetic field [1-11]. Of note, geometries with appropriate obstruction were not necessarily considered in these studies.

Separate obstruction of circular, square, triangular, or other shapes can be applied to controlling the fluid flow and temperature resulting from natural, forced, or mixed convection in a closed or open enclosure. This particular phenomenon has important applications in thermal engineering when fluid flow needs to be restrained or bifurcated. A number of studies have been conducted to explore these phenomena. For example, natural convection in a square enclosure containing a solid body was numerically investigated by House et al. [12]. They observed that the fluid flow and heat transfer were controlled by Rayleigh number, magnetic parameter, obstacle size, and thermal conductivity ratio. Another study on the combined convections, either natural and forced, in a rectangular cavity with a solid cylinder revealed that both heat transfer and temperature in the cavity depended on the governing parameters [13]. In an investigation into the entropy generation for magnetohydrodynamic mixed convection in an open cavity filled with hybrid nanofluid in the presence of an adiabatic square obstacle, the increased magnetic field effects decreased the average Nusselt number and improved the entropy generation [14]. Mehmood et al. [15] analyzed the mixed convection in a lid-driven square cavity with a heated hollow obstacle in the presence of magnetic field. They reported that the magnetic field affected heat transfer and average entropy generation. Later on, Selimefendigil and Oztop [16] numerically studied the mixed convection in a PCM filled cavity in the presence of a rotating cylinder. In their study, the heat

transfer and melting process were found controlling with the cylinder rotation. They also observed 10% more heat transfer in the case of using a large cylinder in clockwise rotation than that while using a smaller one. Then, they [17] used a novel method to visualize the combined effects of the oriented magnetic field and rotating tube bundle. They reported that the heat transfer performance coefficient increased 13% more at a Hartmann number of 5 than that in the non-magnetic field configuration. In addition, the heat transfer performance coefficient was found 52% more while the highest solid volume fraction of CNT nanoparticles was suspended in the base fluid. Chamkha et al. [18] conducted a finite element-based numerical study of mixed convection of CNT-water nanofluid flow in a lid-driven 3D trapezoidal porous cavity with a rotating cone under the effect of magnetic field and found that the aspect ratio of the cone could be an excellent tool for heat transfer enhancement. CNT nanoparticles caused an increase in the average Nusselt and the magnetic field decreased convection. In this regard, it can be concluded that the presence of internal blockage could affect the heat transfer rate and fluid motion. However, the analysis of heat transfer performance affected by irregular surfaces of different geometries did not receive enough attention in these studies.

The irregular surfaces of a complicated structure form additional recirculation regions that can improve the mixing of fluid and heat transfer characteristics, compared to other simple structures. In fact, the wavy surfaces of a complicated geometry can radically improve the heat transfer performance in many engineering systems such as heat exchangers, electronic cooling, nuclear reactors, chemical processing equipment, lubrication systems, food processing, and underground cable systems [19]. The problems of mixed convection and entropy generation in a nanofluid filled wavy cavity equipped with a rotating cylinder were investigated in detail with multiple variations of the configuration [20–21]. Later on, the finite volume approach with SIMLE algorithm was taken into account to examine laminar nanofluid flow and heat transfer in a sinusoidal-wavy channel [22]. Incorporation of nanoparticles with an increase in the pumping power significantly enhanced the heat transfer and decreased the coefficient of skin friction. Makinde and Reddy [23] examined the effect of velocity slip on hydromagnetic peristaltic flow of Casson fluid through an asymmetric channel filled with porous medium and observed that the permeability parameter could increase the size of trapped bolus; however, under the effect of velocity slip, it diminished. Moreover, the velocity and temperature profiles decreased with an increase in the magnetic field and Casson fluid parameters. A numerical investigation of the forced convection and pressure drop in nanofluids flow through a horizontal tube and wavy channel

proved that single-phase models could provide accurate nanofluids transport characteristics through a wavy channel more precisely than two-phase models [24]. By using finite volume approach to analyze the heat transfer mechanism in a corrugated duct, it was observed that enhancement was affected by the corrugated shape of the channel and Reynolds number [25]. Ionescu and Neagu [26] numerically investigated the flow and heat transfer characteristics in a corrugated channel using finite element method. In their study, the thermal boundary layer was found to be thinner in the concave portions of the channel, and the local Nusselt along the lower channel wall increased upon increasing the spacing ratio when the waviness parameter under study is kept constant. The effect of the heat source of different lengths on the phenomenon of heat transfer in a horizontal channel attached to an open trapezoidal cavity was evaluated by Laouira et al. [27]. They noted that local and average Nusselt numbers increased upon increasing the length of heat source. Later on, Al-Farhany et al. [28] extended this study considering the magnetic field effect and demonstrated that the heat transfer rate increased upon increasing Richardson number and decreased under the magnetic field effects.

According to the previous studies, geometrical configuration plays a significant role in the fluid flow and heat transfer behavior. Although numerous studies have been conducted on the mixed convection in different geometries to date, understanding this phenomenon in a nanofluid filled wavy conduit is still challenging. The primary objective of the present study was to numerically examine the mixed convection in a nanofluid filled wavy conduit with a pair of isothermal rotating circular cylinders acting as the obstructions. Simulations were performed based on finite element method. Numerical results were obtained for flow and thermal fields using streamlines, temperature contours, and heat transfer rate. A detailed parametric discussion was also presented based on the obtained results in the following section. In the authors' opinion, this innovative research can be significantly employed in practical applications in thermal engineering fields as a means of enhancing the performance of flow mixing and heat transfer mechanisms, e.g., cooling systems for electronic and micro-electronic devices, solar collectors, industrial heat radiators, heat exchangers, specific heat exchanger for industrial applications such as an engine intercooler system, and so on [19,26,29].

2. Physical model

Figure 1 shows a physical model of the wavy conduit filled with copper oxide-water nanofluid. A pair of rotating cylinders was included in the conduit. Its bottom surface was heated at T_h and the top surface was cooled at T_c , i.e., $T_h > T_c$. Isothermal

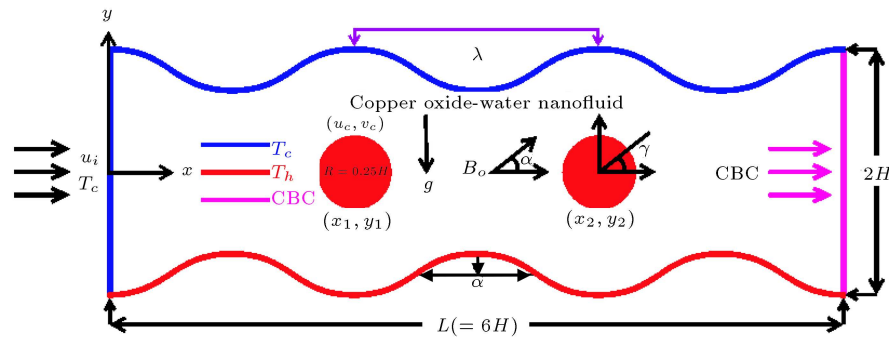


Figure 1. Schematic diagram of the wavy conduit.

Table 1. Thermo-physical properties of water and copper-oxide [30].

Physical properties	Water	Copper-oxide (CuO)
C_p (J/kg.K)	4179	540
ρ (kg/m ³)	997.1	6500
k (W/mK)	0.613	18
β (1/K)	2.1×10^{-4}	0.085×10^{-4}
σ ($\Omega \text{ m}$) ⁻¹	0.05	10^{-10}

temperatures were maintained on these surfaces. All rotating cylinders had a radius of 0.25 H . The thermal condition and rotation speed and direction were identical for the cylinders. The initial conditions for the simulations are as follows:

- Uniform velocity at the inlet: u_i .
- Inlet temperature: T_c .
- Convective boundary condition at the outlet.
- Conduit length: $L = 6H$.
- Conduit height $2H$ whose amplitude was a and wave length λ .
- A uniform magnetic field $\vec{B}_0 = B_x \hat{i} + B_y \hat{j}$ was functionalized at an angle α and its strength was measured by $B_0 = \sqrt{B_x^2 + B_y^2}$.

All the thermo-physical properties of the fluid were considered fixed except density that changed with a change in temperature. Table 1 shows a combination of base fluid and nanoparticles. As dimensional coordinate systems, x -axis and y -axis were assumed to be along the horizontal and vertical directions, respectively. The gravitational acceleration (g) was taken in the negative direction of y -axis, i.e., in the downward direction.

3. Mathematical analysis

Based on both Boussinesq approximation and current physical models, the conservation equations of the flow model can be written as [13–15,31,32]:

$$\frac{\partial u}{\partial x} + \frac{\partial v}{\partial y} = 0, \tag{1}$$

$$u \frac{\partial u}{\partial x} + v \frac{\partial u}{\partial y} = -\frac{1}{\rho_{nf}} \frac{\partial p}{\partial x} + \frac{\mu_{nf}}{\rho_{nf}} \left(\frac{\partial^2 u}{\partial x^2} + \frac{\partial^2 u}{\partial y^2} \right) + \frac{\sigma_{nf}}{\sigma_f} B_0^2 (v \sin \alpha \cos \alpha - u \sin^2 \alpha), \tag{2}$$

$$u \frac{\partial v}{\partial x} + v \frac{\partial v}{\partial y} = -\frac{1}{\rho_{nf}} \frac{\partial p}{\partial y} + \frac{\mu_{nf}}{\rho_{nf}} \left(\frac{\partial^2 v}{\partial x^2} + \frac{\partial^2 v}{\partial y^2} \right) + \frac{1}{\rho_{nf}} [g \beta_{nf} \rho_{nf} (T - T_c)] + \frac{\sigma_{nf}}{\sigma_f} B_0^2 (u \sin \alpha \cos \alpha - v \cos^2 \alpha), \tag{3}$$

$$u \frac{\partial T}{\partial x} + v \frac{\partial T}{\partial y} = \frac{k_{nf}}{(\rho c_p)_{nf}} \left(\frac{\partial^2 T}{\partial x^2} + \frac{\partial^2 T}{\partial y^2} \right), \tag{4}$$

$$k_{s1} \left(\frac{\partial^2 T_{s1}}{\partial x^2} + \frac{\partial^2 T_{s1}}{\partial y^2} \right) + q_1 = 0, \tag{5}$$

$$k_{s2} \left(\frac{\partial^2 T_{s2}}{\partial x^2} + \frac{\partial^2 T_{s2}}{\partial y^2} \right) + q_2 = 0. \tag{6}$$

Here, the estimated properties of nanofluids in these equations (Eqs. (1)–(6)) are presented below [6,9,14,15,33]:

$$\rho_{nf} = (1 - \phi) \rho_f + \phi \rho_s, \tag{7}$$

$$\mu_{nf} = \mu_f (1 + 39.11\phi + 533.9\phi^2), \tag{8}$$

$$(\rho c_p)_{nf} = (1 - \phi) \rho_f (c_p)_f + \phi \rho_s (c_p)_s, \tag{9}$$

$$\beta_{nf} = (1 - \phi) \beta_f + \phi \beta_s, \tag{10}$$

$$k_{nf} = k_f((k_s + 2k_f - 2\phi(k_f - k_s)) / (k_s + 2k_f + \phi(k_f - k_s))), \tag{11}$$

$$\alpha_{nf} = k_{nf} / (\rho c_p)_{nf}, \tag{12}$$

$$\sigma_{nf} = \sigma_f(1 + ((3(\sigma_r - 1)\phi) / ((\sigma_r + 2) - (\sigma_r - 1)\phi))),$$

$$\sigma_r = \sigma_s / \sigma_f. \tag{13}$$

Both static and dynamic mechanisms were taken into account to model the thermal conductivity of nanofluids on the basis of medium theory [34,35]. It is important to note that the dynamic mechanism, viz. Brownian motion of nanoparticles, can significantly contribute to improving the thermal conductivity of nanofluids. However, it was not included in the Maxwell’s thermal conductivity model [6]. In the current study, the Maxwell’s model was extended by incorporating the Brownian motion effect [36], as shown in the following:

$$k_{nf} = \frac{(k_s + 2k_f - 2\phi(k_f - k_s))k_f}{(k_s + 2k_f + \phi(k_f - k_s))} + \frac{\phi \rho_s c_{p,s}}{2} \sqrt{\frac{K_B T_{ref}}{3\pi d_s \mu_f}}. \tag{14}$$

Physical model-based boundary conditions are:

On the bottom wavy surface [19]:

$$u = 0, \nu = 0, T = T_h; \quad -H + a \{1 - \cos(2\pi x/\lambda)\} \\ 0 \leq x \leq L. \tag{15}$$

On the top wavy surface:

$$u = 0, \nu = 0, T = T_c; \quad H - a \{1 - \cos(2\pi x/\lambda)\} \\ 0 \leq x \leq L. \tag{16}$$

At the inlet port:

$$u = u_i, \nu = 0, T = T_c, \quad 0 \leq y \leq L/3. \tag{17}$$

At the outlet port:

$$p = 0, \quad \frac{\partial u}{\partial x} = \frac{\partial v}{\partial x} = \frac{\partial T}{\partial x} = 0, \quad 0 \leq y \leq L/3. \tag{18}$$

On the cylinder surfaces:

$$u_c = \frac{u_p}{u_i} \sin \gamma, \quad v_c = \frac{u_p}{u_i} \cos \gamma, \tag{19}$$

where the peripheral speed is $u_p = \omega R$.

At the solid-fluid interface of the cylinders:

$$u = 0, \nu = 0, \text{ and } \left(\frac{\partial T_{nf}}{\partial n}\right) = K_i \left(\frac{\partial T_s}{\partial n}\right), \\ i = 1, 2. \tag{20}$$

A set of dimensionless variables (in Eq. (21)) was considered in this study to transform the governing equations into the dimensionless form.

$$X = \frac{x}{H}, \quad Y = \frac{y}{H}, \quad U = \frac{u}{u_i}, \\ V = \frac{v}{u_i}, \quad P = \frac{p}{\rho_{nf} u_i^2}, \quad \theta = \frac{T - T_c}{T_h - T_c}, \\ \text{and } \theta_s = \frac{T_s - T_c}{T_h - T_c}. \tag{21}$$

Therefore, converted non-dimensional governing equations are:

$$\frac{\partial U}{\partial X} + \frac{\partial V}{\partial Y} = 0, \tag{22}$$

$$U \frac{\partial U}{\partial X} + V \frac{\partial U}{\partial Y} = -\frac{\partial P}{\partial X} + \frac{\nu_{nf}}{\nu_f} \frac{1}{Re} \left(\frac{\partial^2 U}{\partial X^2} + \frac{\partial^2 U}{\partial Y^2}\right) \\ + \frac{\rho_f \sigma_{nf}}{\rho_{nf} \sigma_f} \frac{Ha^2}{Re} (V \sin \alpha \cos \alpha - U \sin^2 \alpha), \tag{23}$$

$$U \frac{\partial V}{\partial X} + V \frac{\partial V}{\partial Y} = -\frac{\partial P}{\partial Y} + \frac{\nu_{nf}}{\nu_f} \frac{1}{Re} \left(\frac{\partial^2 V}{\partial X^2} + \frac{\partial^2 V}{\partial Y^2}\right) \\ + \frac{(\rho\beta)_{nf}}{(\rho_f \beta_f)} \frac{\rho_f Gr}{\rho_{nf} Re^2} \theta + \frac{\rho_f \sigma_{nf}}{\rho_{nf} \sigma_f} \frac{Ha^2}{Re} \\ (U \sin \alpha \cos \alpha - V \cos^2 \alpha), \tag{24}$$

$$U \frac{\partial \theta}{\partial X} + V \frac{\partial \theta}{\partial Y} = \frac{\alpha_{tnf}}{\alpha_{tf}} \frac{1}{Re Pr} \left(\frac{\partial^2 \theta}{\partial X^2} + \frac{\partial^2 \theta}{\partial Y^2}\right), \tag{25}$$

$$\left(\frac{\partial^2 \theta_{s1}}{\partial X^2} + \frac{\partial^2 \theta_{s1}}{\partial Y^2}\right) + Q_1 = 0, \tag{26}$$

$$\left(\frac{\partial^2 \theta_{s2}}{\partial X^2} + \frac{\partial^2 \theta_{s2}}{\partial Y^2}\right) + Q_2 = 0. \tag{27}$$

The corresponding boundary conditions take the following dimensionless forms:

On the bottom wavy surface:

$$U = 0, V = 0, \theta = 0; \quad -H + a \{1 - \cos(2\pi X/\lambda)\}, \\ 0 \leq X \leq L. \tag{28}$$

On the top wavy surface:

$$U = 0, V = 0, \theta = 0; \quad H - a \{1 - \cos(2\pi X/\lambda)\},$$

$$0 \leq X \leq L. \tag{29}$$

At the inlet port:

$$U = 1, \quad V = 0, \quad \theta = 0, \quad 0 \leq Y \leq L/3. \tag{30}$$

At the outlet port:

$$P = 0, \quad \frac{\partial U}{\partial X} = \frac{\partial V}{\partial X} = \frac{\partial \theta}{\partial X} = 0, \quad 0 \leq Y \leq L/3. \tag{31}$$

On the cylinder surfaces:

$$U_c = Sr \sin \gamma \quad V_c = Sr \cos \gamma,$$

where:

$$Sr = \frac{U_{ps}}{U}. \tag{32}$$

At the solid and fluid interface of cylinders:

$$\left(\frac{\partial \theta}{\partial N} \right)_{nf} = K_i \left(\frac{\partial \theta_s}{\partial N} \right)_s, \quad i = 1, 2. \tag{33}$$

3.1. Descriptions of the important parameters

3.1.1. Nusselt number

Nusselt number was used to measure the heat transfer rate from the heated surface, which is defined in the dimensional form as [37,38]:

$$Nu = \frac{h H}{k_f}. \tag{34}$$

The heat transfer coefficient (h) and thermal conductivity of nanofluid can be defined using heat flux as [37,38]:

$$h = \frac{q_w}{T_h - T_c}, \tag{35}$$

and:

$$k_{nf} = -\frac{q_w}{\partial T / \partial y}. \tag{36}$$

Based on Eqs. (34)–(36) and dimensionless quantities (Eq. (21)) in this study, Nusselt number is defined as [37,38]:

$$Nu = -\frac{k_{nf}}{k_f} \frac{\partial \theta}{\partial Y}, \tag{37}$$

$$Nu_{av} = \frac{1}{S} \int_0^S Nu \sqrt{1 + (dy/dx)^2} dx, \tag{38}$$

where S represents the length of bottom surface and (k_{nf}/k_f) is calculated using Eq. (14).

3.1.2. Average temperature

The following expression was used to evaluate the average temperature inside the channel [39]:

$$\theta_{av} = \int (\theta/\bar{V}) d\bar{V}, \tag{39}$$

where \bar{V} is the conduit volume.

3.2. Numerical procedure

The governing equations (Eqs. (22)–(27)) related to the boundary conditions (Eqs. (28)–(33)) were solved by using finite element method. The numerical procedure demands the application of the method available in [40,41]. Galerkin weighted residual technique was considered in the current simulation to convert the aforementioned equations into a set of integral equations [42]. They were transferred into nonlinear algebraic equations using Gauss quadrature method [43], which was necessarily modified by imposing the relevant boundary conditions. The obtained nonlinear algebraic equations were simplified into linear algebraic equations [44,45]. The simplified equations were solved using triangular factorization technique [46]. Application of this simulation procedure is also available in our studies [47,48]. However, details of this procedure are not presented here.

3.3. Mesh analysis

Mesh analysis is a procedure that divides a geometric domain into a set of sub-domains considering triangular or quadrilateral elements for 2D geometric domain called finite elements. It is a discrete presentation of computational domain where the dependent variables of a problem are to be solved. In the case of finite element method, the mesh analysis of complicated geometrics makes it a powerful and versatile analytical tool for solving the engineering problems faced in practical applications [49]. The mesh configuration of the present study is given in Figure 2.

The dependency of the current numerical results on meshing was tested with respect to the average Nusselt number calculated for different mesh sizes [31]. The exemplary results of this grid sensitivity analysis are presented in Table 2. A mesh size of 14193 nodes and 27504 elements was found appropriate to obtain the mesh independent solution to the present problem.

3.4. Model validation

To validate the current model, the numerical procedure was employed to solve the problems of mixed

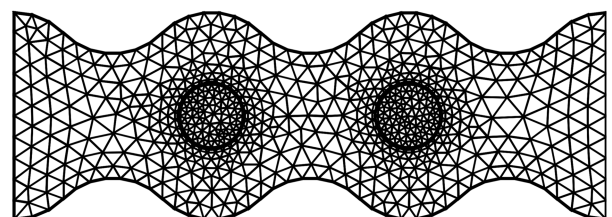


Figure 2. Presentation of 2D triangular meshes in the wavy conduit.

Table 2. Grid sensitivity test at $Pr = 6.2$, $Re = 20$, $Ha = 20$, $\alpha = 45^\circ$, and $\phi = 1\%$.

Nodes	4882	8610	11443	14193	17310
(elements)	(9354)	(16590)	(22130)	(27504)	(33610)
Nu_{av}	9.20985	9.32724	9.38528	9.42472	9.44154

Table 3. Comparison of average Nusselt number ($Ra =$ Rayleigh number and $K =$ thermal conductivity ratio).

Ra	K	Present work	House et al. [12]	Rahman et al. [13]	$ ((a - b)/b) \times 100 $	$ ((a - c)/c) \times 100 $
0	0.2	0.7072	0.7063	0.7071	0.127	0.0141
0	1.0	1.0000	1.0000	1.0000	0.000	0.000
0	5.0	1.4144	1.4125	1.4142	0.134	0.0141
10^5	0.2	4.6218	4.6239	4.6337	0.045	0.2567
10^5	1.0	4.5020	4.5061	4.5037	0.091	0.0377
10^5	5.0	4.3174	4.3249	4.3190	0.173	0.0370

convection and natural convection flow in varying geometric configurations [12,13,28]. These problems were resolved earlier through different numerical codes.

- a) House et al. [12] examined heat transfer enhancement for natural convection in a square cavity with a centered heat conducting obstacle. The control volume method was used to simulate the governing equations. We exercised the present code to solve the problem posed by House et al. [12] and then compared them with existing results given in [12].
- b) Rahman et al. [13] numerically investigated the free and forced convection in a rectangular cavity equipped with solid cylinder using Galekin weighted residual finite element method. For further verification, the present code is used to solve the problem [13] and then, the results are compared with our results.
- c) Al-Farhany et al. [28] simulated the laminar mixed convection flow in a horizontal channel with an open trapezoidal enclosure under the effect of magnetic field. We simulated the identical problem of [28] and compared our simulated results with those available in [28].

The comparative results are presented in Table 3 and Figure 3. The maximum deviation was less

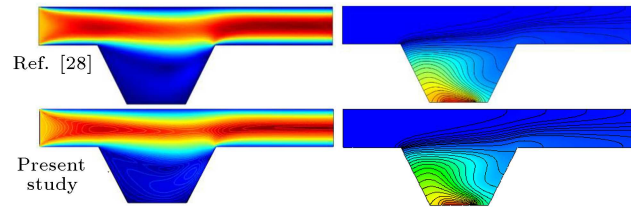


Figure 3. Validation of the present code against the numerical results presented in [28]: streamlines (left) and isotherms (right).

than 1% in Table 3. The close agreement between the current results and similar findings reported in the previous studies validates the present simulation methodology.

4. Results and discussion

The current research performed a numerical simulation of convective flow of nanofluid in a wavy conduit with a pair of rotating cylinders subjected to an inclined magnetic field. The objective was to evaluate the effects of the selected number of physical parameters on the flow structure and temperature fields. The ranges of values for the governing parameters considered for the simulations are presented in Table 4.

The findings of this study were presented using

Table 4. The range of values for the governing parameters.

Parameter	Lowest values	Highest values
Reynolds number	20	200
Nanoparticle volume fraction	0%	5%
Magnetic field parameter	0	50
Magnetic inclination angle	0°	180°
Speed ratio	-2	+2
Prandtl number for the base fluid	6.2	6.2

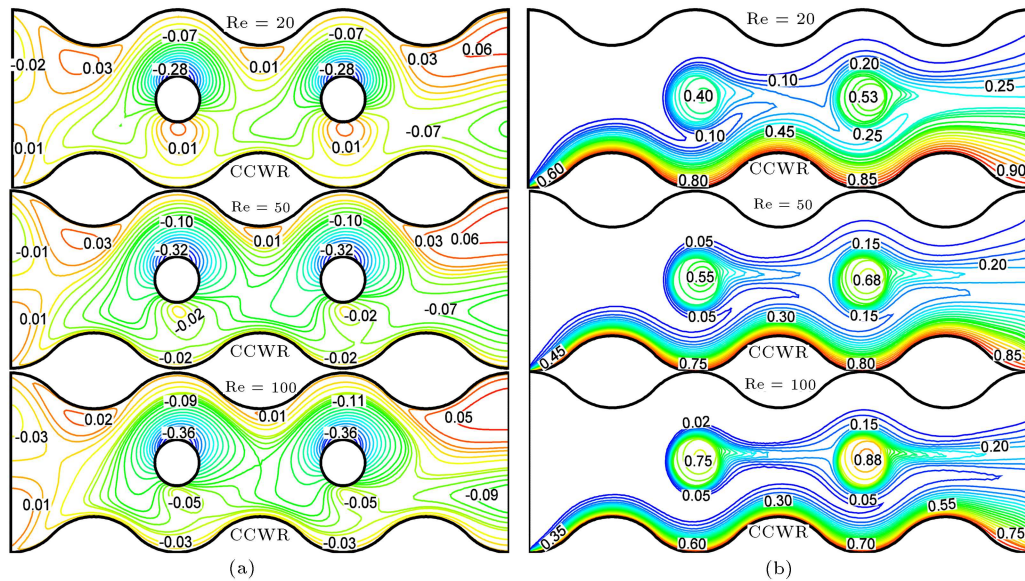


Figure 4. Plots showing the streamlines (a) and isotherms (b) with respect to ($Pr = 6.2$, $Ha = 20$, $\alpha = 45^\circ$, and $\phi = 1\%$).

streamlines and isotherm contours. The results were also analyzed from a physical point of view using the values of average Nusselt number.

4.1. Reynolds number (Re)

The effect of Reynolds number on streamlines and isotherms is illustrated in Figure 4 with the cylinders undergoing Counter Clock Wise Rotation (CCWR). As shown in Figure 4(a), a pair of vortices was formed on the upper surface of the cylinders. However, each of these intersected with the cylinder prior to their complete development. A couple of secondary vortices were also formed on lower surfaces of the cylinders which were weaker in strength and smaller in size than the upper vortices. As the strength of flow circulation increased, the streamlines became condensed from the cylinders to the upper wavy surface of the conduit with rising Re . It was, most likely, because higher Re led to greater fluid inertia, hence an increase in both magnitude and concentration of streamlines. Moreover, half-done circulations were formed near the end of the conduit as a result of the effects of governing parameters and imposed boundary conditions. The streamlines near the wavy surface became curvy from inlet to outlet of the conduit. Significant changes were also observed in the distribution of the streamlines for changes in Re . On the other hand, as shown in Figure 4(b), the isotherms are densely distributed over the heated surface and rotating cylinders, indicating that the heat transfer begins from these regions. Ring-shaped circulations were also formed within and around the cylinders for the combined effect of physical parameters and imposed thermal conditions. As Re increased in Figure 4(b), the isotherms in the direction of flow were squeezed towards the bottom surface and cylin-

ders. Reducing the thickness of the thermal boundary layer increased the forced convection effects and heat transfer rate as well. Of note, the temperature near the center of the cylinders increased upon increasing Re , mainly because the thermal conductivity of the solid domains was conversely varied with respect to Reynolds number, thus causing a reduction in heat flux from each rotating heat source to the surrounding fluid. The counter clockwise rotation also moved the isotherms to the upward direction near the rear of the heat sources as well as the channel.

4.2. Nanoparticle concentration (ϕ)

Streamline plots for different concentrations of nanoparticles in the base fluid are presented in Figure 5(a). For this kind of computations, the cylinders were maintained in spinning states (CCWR) while other parameters were kept constant. As shown in Figure 5(a), the two vortices were formed next to each rotating cylinder. The upper one was much stronger and larger, i.e., more concentrated, than the lower one. The magnitude of the flow field was greater in the base fluid than that in the nanofluid of 1% nanoparticles. Further increase in nanoparticle concentration up to 5% did not cause any significant change in the streamline distribution within the channel; however, increasing the concentration of nanoparticles reduced the magnitude of flow circulation. The physics behind it is that higher concentration of nanoparticles increases not only the effective density of nanofluid (Eq. (7)), but also its viscosity (Eq. (8)) which generates clogging force inside that channel which retards the fluid motion. Moreover, circulations under the rotating cylinder are intensified with higher strength in the case of greater volume fraction, which is indicative of extra heat transfer

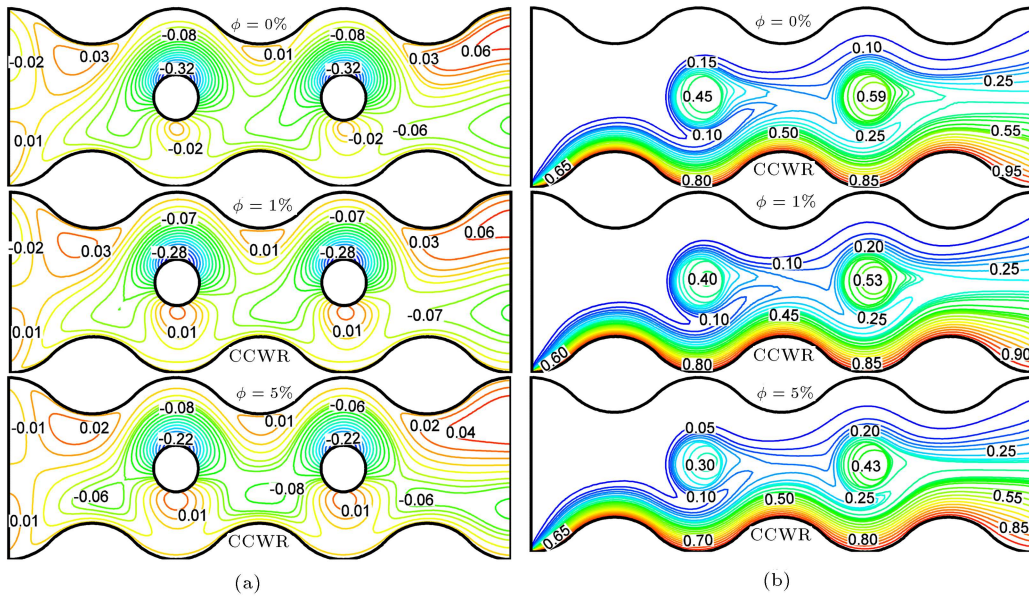


Figure 5. Plots showing the streamlines (a) and isotherms (b) with respect to ϕ ($Pr = 6.2, Re = 20, Ha = 20$, and $\alpha = 45^\circ$).

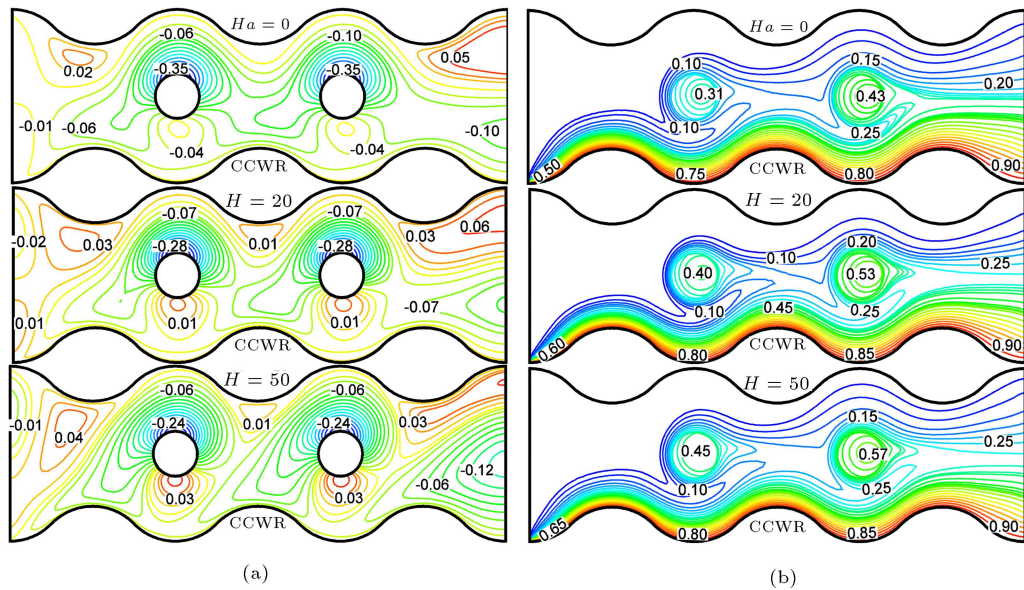


Figure 6. Plots showing the streamlines (a) and isotherms (b) with respect to Ha ($Pr = 6.2, Re = 20, \alpha = 45^\circ$, and $\phi = 1\%$).

there. Figure 5(b) represents the isotherm contours for different concentrations of nanoparticles. According to this figure, when nanoparticles are not amalgamated in the base fluid ($\phi = 0\%$), a considerable temperature pattern appears over the hot surfaces. This, in turn, suggests that isotherm contours were emanated from the heated surfaces. When nanoparticles of 1% were suspended into the base fluid, the isotherms maintained similar patterns at different temperatures. At the same time, high temperature near the center of the cylinders was reduced. Further increase in the concentration of nanoparticles (up to 5%) in the base fluid did not result

in any significant change in distribution of isotherms except in the core regions of the cylinders, mainly because the effective thermal conductivity of the fluid domain (Eq. (14)) and solid domain increased by the suspended nanoparticles.

4.3. Strength of magnetic field (Ha)

Figure 6 presents the flow circulations and temperature distributions for different values of Ha as well as fixed values of the remaining parameters with streamline and isotherm plotting. According to Figure 6(a), the magnetic field strength could considerably affect

modification of the streamline distribution in the flow path and reduce the flow strength of the recirculation cells within the conduit. This occurred as a result of the interaction of the magnetic force with the buoyancy force and fluid inertia to produce Lorentz force. Consequently, the increased Lorentz force for higher magnetic field effects suppressed the fluid motion within the conduit. This is the reason why the formation of convection circulations in the direction of flow changed significantly at higher magnetic strength ($Ha = 50$). Therefore, it can be concluded that the magnetic field can regulate the shape and strength of flow circulation through a channel. Figure 6(b) demonstrates the effects of Ha on isotherm contours at certain values of the controlling parameters while the cylinders are in motion. The isotherm pattern did not change considerably under the magnetic field effect. Moreover, in the case of large Ha , the high temperature within the heat sources increased. The physics behind it is that the interaction of the magnetic force with buoyancy force can produce an additional degree of temperature inside the channel, thus causing a reduction in the heat transfer rate from sources.

4.4. Speed ratio (Sr)

Figure 7 shows the streamlines and temperature contours at different speed ratios while other parameters are assumed constant. The negative and positive values

of Sr are indicative of CWR and CCWR, respectively. Similarly, $Sr = 0$ refers to the stationary state of the cylinders. As demonstrated in Figure 7(a), a pair of primary symmetrical vortices of equal magnitude was produced besides the stationary cylinders. In addition, secondary complete circulations of equal strength were observed in the conduit. Moreover, symmetrical incomplete vortices were also produced near the inlet and outlet of the conduit. Formation of this type of vortices is indicative of an equal rate of heat transfer from both sides of each heat source. When the cylinders rotated at a speed ratio of 1 (as shown in Figure 5(a) at $Re = 20$), the primary vortices on the upper surface of the cylinder became stronger with higher concentration. At the same time, the vortices under the cylinders turned out to be weaker due to the reduced number of cells and flow strength. As the speed ratio increased further to 2, the rotational speed dominated the flow field by producing elongated convection circulations with greater strength. Consequently, more convective heat was released from the upper surface of the rotating cylinders. Wavy streamlines were also visible near the bottom surface of the channel. On the contrary, the vortices on the upper surface of cylinders turned out to be weaker and smaller in size due to the formation of stronger convection cells when Sr increased up to -1 . In other words, $Sr = -1$ led to a higher convective heat transfer on the lower surface. Upon further

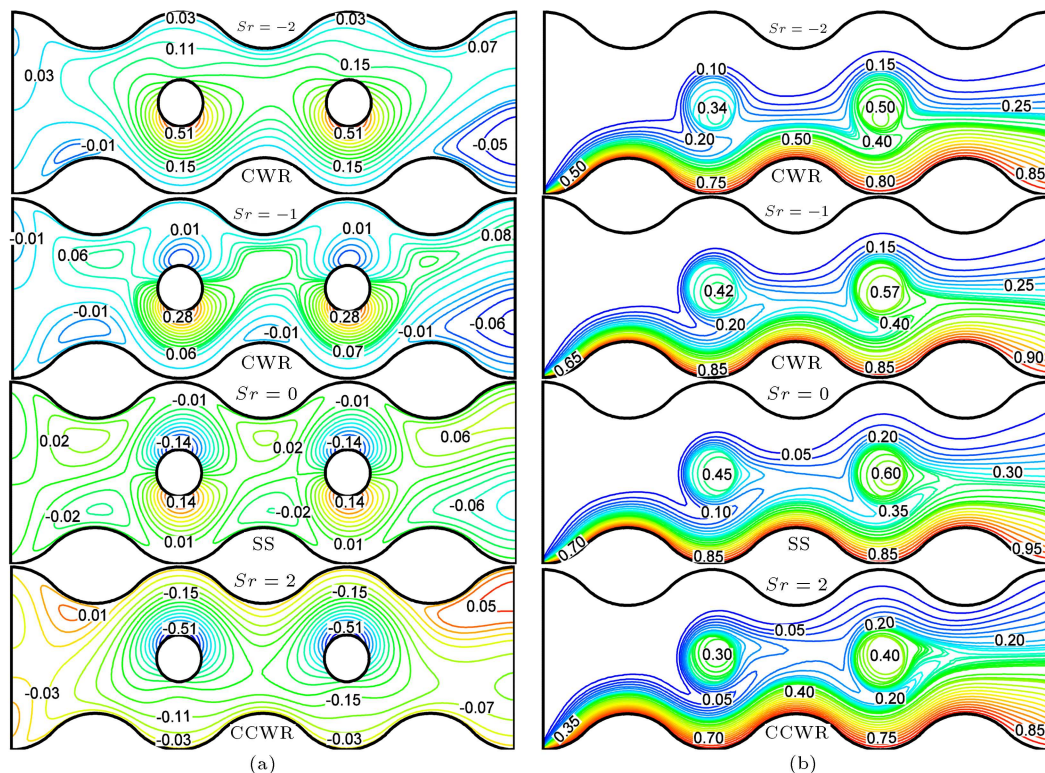


Figure 7. Plots showing the streamlines (a) and isotherms (b) with respect to Sr ($Pr = 6.2$, $Re = 20$, $Ha = 20$, $\alpha = 45^\circ$, and $\phi = 1\%$).

increase in the speed ratio up to -2 , the lower vortices were intensified in large shapes. In this case, wavy streamlines were also visible near the upper surface of the channel. On the other hand, an increase in the speed ratio notably modified the temperature contours (shown in Figures 7(b) and 5(b) at $Re = 20$). The temperature near the center of cylindrical heat sources decreased with an increase in the value of Sr mainly because higher speed ratio accelerated the fluid motion throughout the conduit, thus leading to higher rate of heat transfer as expected.

4.5. Heat transfer

Figures 8–10 show the effects of the magnetic field on the variations in the average Nusselt number and temperature in the range of Re , ϕ , and α . The solid

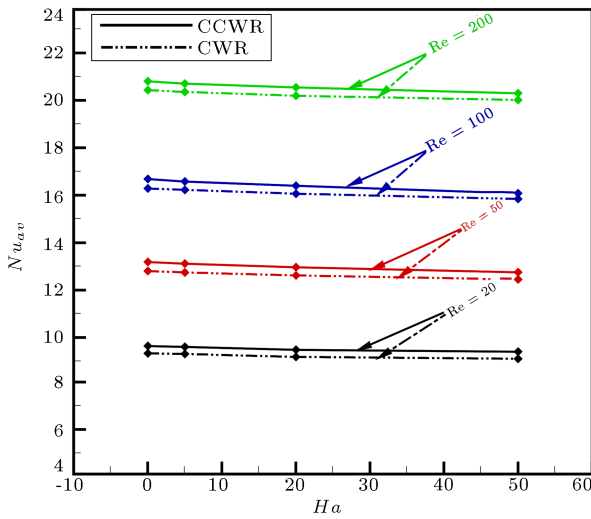


Figure 8. Plots showing the average Nusselt number for CCWR and CWR of the cylinders ($Ha =$ variable, $Re =$ variable, $Pr = 6.2$, $\alpha = 45^\circ$, and $\phi = 1\%$).

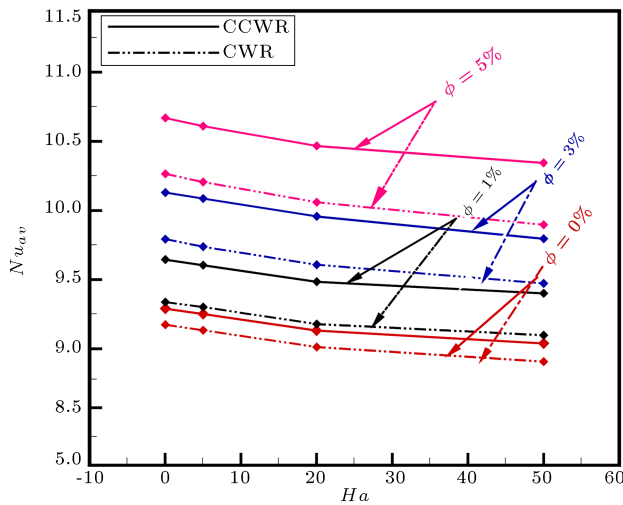


Figure 9. Plots showing the average Nusselt number for CCWR and CWR of the cylinders ($Ha =$ variable, $\phi =$ variable, $Pr = 6.2$, $Re = 20$, and $\alpha = 45^\circ$).

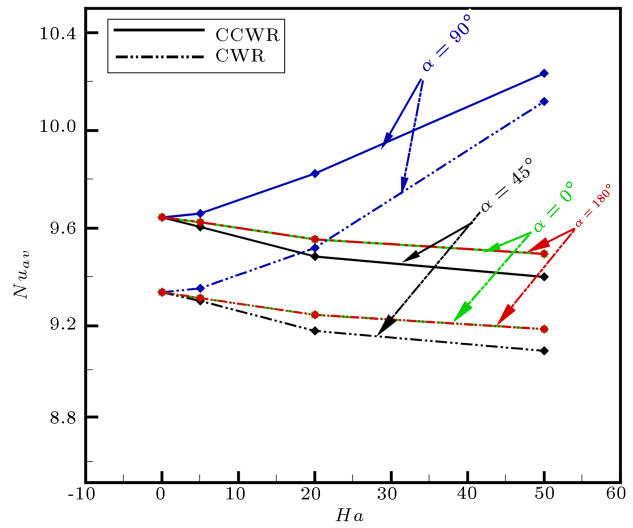


Figure 10. Plots showing the average Nusselt number for CCWR and CWR of the cylinders ($Ha =$ variable, $\alpha =$ variable, $Pr = 6.2$, $Re = 20$, and $\phi = 1\%$).

and dashed lines correspond to the values of Counter Clockwise Rotation (CCWR) and Clockwise Rotation (CWR) of the heat sources, respectively. As shown in Figure 8, the average Nusselt number decreased as the strength of magnetic field increased, which was already expected since the magnetic force was the source of temperature in the flow field. It was also found the heat transfer rate was reduced by 2.59% and Ha varied from 0 to 50. In addition, the heat transfer rate increased rapidly as the values of Re increased. Of note, a higher value was obtained for the average Nusselt number in CCWR than that in CWR. The numerical results confirmed a 115.72% increase in the heat transfer rate due to variations in Re from 20 to 200 in the CCWR in the absence of magnetic field effect ($Ha = 0$), and it was 110.50% while the magnetic field of strength of 50 was placed at an angle of 45° . Figure 9 confirms the sufficient heat transfer enhancement for incorporation of nanoparticles into the base fluid water. Moreover, in the absence of magnetic field, the average Nusselt number increased up to 16.30% and 11.89%, respectively, as the volume fraction increased from 0% to 5% in CCWR and CWR. The corresponding values when exposed to the magnetic field of 50 in strength at an angle of 45° were 12.77% and 7.89%, respectively. Figure 10 demonstrates a typical plotting of the heat transfer rate and mean temperature for different amounts of magnetic field strength and inclination angles. Of note, the average Nusselt number had the same values at $\alpha = 0^\circ$ and $\alpha = 180^\circ$ for all Ha 's. These values were at maximum and minimum, respectively, while the magnetic field was placed at angles of 90° and 45° .

4.6. Comparative results

Figure 11 represents the comparative results of the heat transfer rate using average Nusselt number for

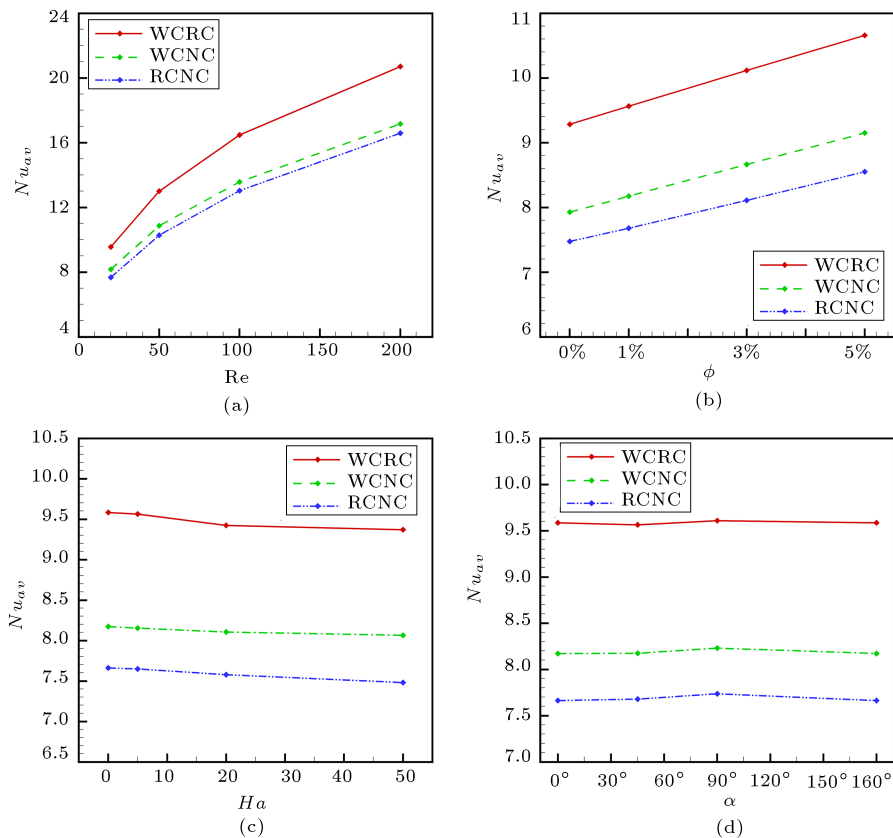


Figure 11. Plots showing the average Nusselt number for different Re (a), ϕ (b), Ha (c), and α (d).

different configurations modeled as Wavy Conduit with Rotating Cylinders (WCRC), Wavy Conduit with No Cylinders (WCNC), and Rectangular Channel with No Cylinders (RCNC). As shown in Figure 11, in the case of WCRC, compared to WCNC and RCNC, the heat transfer rate accelerated significantly due to an increase in Re and ϕ . In addition, the heat transfer rates in RCNC, WCNC, and WCRC increased by 115.99%, 123.54%, and 169.69%, respectively, depending on the variations in Re (20–200). A similar behavior was observed for variations in the magnetic field effect and inclination angle. In particular, heat transfer rates in WCRC and WCNC increased by 51.68% and 5.40% more than that in RCNC while magnetic field was placed at an angle of 0° . Accordingly, the values for the same parameters were 54.10% and 6.81% while magnetic field was placed at an angle of 90° .

5. Conclusions

The present study numerically investigated mixed convection in a wavy conduit with a pair of rotating cylindrical heat sources in the presence of a magnetic field. To this end, the finite element method was employed to solve the governing equations. Numerical code was also validated through an appropriate comparison between the numerical and experimental

results. The effects of Reynolds number, nanoparticles concentration, Hartmann number, and inclination of the magnetic field on the flow and temperature behaviors within the wavy conduit were systematically examined. The major findings of this analysis are summarized in the following:

- Fluid flow represented by the streamlines accelerated significantly upon increasing the Reynolds number in the presence of cylindrical heat sources and declined with the addition of nanoparticles and higher strength amounts of magnetic field;
- Thermal field represented by the isotherm distribution was sensitive to variations in Re and the presence of heat sources; however, it was insensitive to variations in ϕ and Ha ;
- Heat transfer was enhanced with an increase in Re and ϕ , whereas it was reduced with increase in Ha at an angle of 45° ;
- Average temperature decreased upon increasing Re and increased upon increasing Ha and ϕ ;
- Magnetic inclination angles exhibited typical behavior in terms of heat transfer rate and average temperature, as well;
- Compared to other cases, the maximum heat trans-

fer was ensured, while magnetic field was set to an angle of 90° ;

- The speed ratio had a significant effect on modulating the streamlines and isotherms distribution;
- Efficiency of the heat transfer mechanism was found optimum while using rotating cylinders rather than their absence. There was a similar observation in the case of wavy surface compared to rectangular surfaces;
- Heat transfer was maximum in the counterclockwise rotation of the cylinders compared to the clockwise rotation.

The present study was conducted to introduce the sophisticated applications of the improved designs and suitable combination of significant parametric ranges to enhance the cooling efficiency of thermal equipment. Since we completed the present investigation numerically, experimental investigation is required for further validation of the present simulated findings.

Nomenclature

a	Amplitude of the wavy conduit (m)
B_0	Magnitude of the applied magnetic field (Wb/m ²)
c_p	Specific heat at constant pressure (J/kg.K)
d_s	Nanoparticle diameter (nm)
g	Gravitational acceleration (m/s ²)
Gr	Grashof number ($g\beta_f(T_h - T_c)H^3/\nu_f^2$)
H	Height of the wavy conduit (m)
h	Heat transfer coefficient (W/m ² .K)
Ha	Hartmann number ($B_0L\sqrt{\sigma_f/\mu_f}$)
L	Length of the wavy conduit (m)
k	Thermal conductivity (W/m.K)
K_B	Boltzmann constant (J/K)
K_i	Thermal conductivity ratio
N	Number of undulation
n	Normal direction
Nu_{av}	Average Nusselt number
Pr	Prandtl number (ν_f/α_{tf})
p	Dimensional pressure (N/m ²)
P	Dimensionless pressure
q_w	Heat flux (W/m ²)
Q	Dimensionless heat generation
R	Radius of the cylinder (K)
Re	Reynolds number (u_iL/ν_f)
T	Dimensional temperature (K)

T_{ref}	Reference temperature (K)
Sr	Speed ratio
u, v	Dimensional velocity components (m/s)
U, V	Dimensionless velocity components
x, y	Dimensional coordinates (m)
X, Y	Dimensionless coordinates

Greek symbols

α_t	Thermal diffusivity (m ² /s)
β	Thermal expansion coefficient (1/K)
α	Magnetic inclination angle
λ	Dimensionless wave length (m)
ϕ	Volume fraction of nanoparticles
θ	Dimensionless temperature ($(T - T_c)/(T_h - T_c)$)
μ	Dynamic viscosity (kg/m.s)
ν	Kinematic viscosity (m ² /s)
ρ	Density (kg/m ³)
σ	Electrical conductivity
ω	Angular rotational velocity (m/s)

Subscripts

f	Base fluid
h	Hot
c	Cold
nf	Nanofluid
r	Ratio
s	Solid

Abbreviations

CBC	Convective Boundary Condition
CWR	Clockwise Rotation
CCWR	Counter Clockwise Rotation
SS	Stationary State
PS	Peripheral Speed
WCRC	Wavy Conduit with Rotating Cylinders
WCNC	Wavy Conduit without Cylinders
RCNC	Rectangular Conduit without Cylinders

References

1. Basak, T., Roy, S., Sharma, P.K., et al. "Analysis of mixed convection flows within a square cavity with uniform and non-uniform heating of bottom wall", *International Journal of Thermal Sciences*, **48**(5), pp. 891–912 (2009).

2. Oztop, H.F., Al-Salem, K., and Pop, I. “MHD mixed convection in a lid-driven cavity with corner heater”, *International Journal of Heat and Mass Transfer*, **54**(15–16), pp. 3494–3504 (2011).
3. Chatterjee, D. “MHD mixed convection in a lid-driven cavity including a heated source”, *Numerical Heat Transfer, Part A: Applications*, **64**(3), pp. 235–254 (2013).
4. Hossain, M.S. and Alim, M.A. “MHD free convection within trapezoidal cavity with non-uniformly heated bottom wall”, *International Journal of Heat and Mass Transfer*, **69**, pp. 327–336 (2014).
5. Sivasankaran, S., Malleswaran, A., Bhuvaneshwari, M., et al. “Hydro-magnetic mixed convection in a lid-driven cavity with partially thermally active walls”, *Scientia Iranica*, **24**(1), pp. 153–163 (2017).
6. Maxwell, J.C., *A Treatise on Electricity and Magnetism II*, Cambridge, UK: Oxford University Press (1873).
7. Choi, S.U. “Nanofluids: from vision to reality through research”, *Journal of Heat Transfer*, **131**(3), 033106 (2009).
8. Fereidoon, A., Saedodin, S., Hemmat Esfe, M., et al. “Evaluation of mixed convection in inclined square lid-driven cavity filled with $\text{Al}_2\text{O}_3/\text{water}$ nanofluid”, *Engineering Applications of Computational Fluid Mechanics*, **7**(1), pp. 55–65 (2013).
9. Hussain S., Mehmood K., and Sagheer M. “MHD mixed convection and entropy generation of water-alumina nanofluid flow in a double lid driven cavity with discrete heating”, *Journal of Magnetism and Magnetic Materials*, **419**, pp. 140–155 (2016).
10. Kareem, A.K., Mohammed, H.A., Hussein, A.K., et al. “Numerical investigation of mixed convection heat transfer of nanofluids in a lid-driven trapezoidal cavity”, *International Communications in Heat and Mass Transfer*, **77**, pp. 195–205 (2016).
11. M’hamed, B., Sidik, N.A.C., Yazid, M.N.A.W.M., et al. “A review on why researchers apply external magnetic field on nanofluids”, *International Communications in Heat and Mass Transfer*, **78**, pp. 60–67 (2016).
12. House J.M., Beckermann C., and Smith T.F. “Effect of a centered conducting body on natural convection heat transfer in an enclosure”, *Numer Heat Transf*, **18**(2), pp. 213–25 (1990).
13. Rahman, M.M., Alim, M.A. and Mamun, M.A.H. “Finite element analysis of mixed convection in a rectangular cavity with a heat-conducting horizontal circular cylinder”, *Nonlinear Analysis: Modelling and Control*, **14**(2), pp. 217–247 (2009).
14. Hussain, S., Ahmed, S.E., and Akbar, T. “Entropy generation analysis in MHD mixed convection of hybrid nanofluid in an open cavity with a horizontal channel containing an adiabatic obstacle”, *International Journal of Heat and Mass Transfer*, **114**, pp. 1054–1066 (2017).
15. Mehmood, K., Hussain, S., and Sagheer, M. “Mixed convection in alumina-water nanofluid filled lid-driven square cavity with an isothermally heated square blockage inside with magnetic field effect: Introduction”, *International Journal of Heat and Mass Transfer*, **109**, pp. 397–409 (2017).
16. Selimefendgil, F. and Öztöp, H.F. “Mixed convection in a PCM filled cavity under the influence of a rotating cylinder”, *Solar Energy*, **200**, pp. 61–75 (2020).
17. Selimefendgil, F. and Öztöp, H.F. “Hydro-thermal performance of CNT nanofluid in double backward facing step with rotating tube bundle under magnetic field”, *International Journal of Mechanical Sciences*, **185**, 105876 (2020).
18. Chamkha, A.J., Selimefendgil, F., and Oztöp, H.F. “Effects of a rotating cone on the mixed convection in a double lid-driven 3D porous trapezoidal nanofluid filled cavity under the impact of magnetic field”, *Nanomaterials*, **10**(3), p. 449 (2020).
19. Shenoy, A., Sheremet, M., and Pop, I., *Convective Flow and Heat Transfer from Wavy Surfaces: Viscous Fluids, Porous Media and Nanofluids*, New York: CRC Press (2016).
20. Alsabery, A., Ismael, M., Chamkha, A., et al. “Numerical investigation of mixed convection and entropy generation in a wavy-walled cavity filled with nanofluid and involving a rotating cylinder”, *Entropy*, **20**(9), p. 664 (2018).
21. Alsabery, A.I., Tayebi, T., Chamkha, A.J., et al. “Effect of rotating solid cylinder on entropy generation and convective heat transfer in a wavy porous cavity heated from below”, *International Communications in Heat and Mass Transfer*, **95**, pp. 197–209 (2018).
22. Ahmed, M.A., Yusoff, M.Z., and Shuaib, N.H. “Numerical investigation on the nanofluid flow and heat transfer in a wavy channel”, *Engineering Applications of Computational Fluid Dynamics*, Springer, Cham., pp. 145–167 (2015).
23. Makinde, O.D. and Reddy, M.G. “MHD peristaltic slip flow of Casson fluid and heat transfer in channel filled with a porous medium”, *Scientia Iranica*, **26**(4), pp. 2342–2355 (2019).
24. Albojamal, A., Hamzah, H., Haghghi, A., et al. “Analysis of nanofluid transport through a wavy channel”, *Numerical Heat Transfer, Part A: Applications*, **72**(12), pp. 869–890 (2017).
25. Tokgöz, N., Alıç, E., Kaşka, Ö. and Aksot, M.M. “The numerical study of heat transfer enhancement using Al_2O_3 -water nanofluid in corrugated duct application”, *Journal of Thermal Engineering*, **4**(3), pp. 1984–1997 (2018).
26. Ionescu, V. and Neagu, A.A. “Numerical modelling of fluid flow and heat transfer in a corrugated channel for heat exchanger applications”, *Procedia Manufacturing*, **22**, pp. 634–641 (2018).

27. Laouira, H., Mebarek-Oudina, F., Hussein, A.K., Kolsi, L., Merah, A., and Younis, O. "Heat transfer inside a horizontal channel with an open trapezoidal enclosure subjected to a heat source of different lengths", *Heat Transfer Asian Research*, **49**(1), pp. 406–423 (2020).
28. Al-Farhany, K., Alomari, M.A., and Faisal, A.E. "Magnetohydrodynamics mixed convection effects on the open enclosure in a horizontal channel heated partially from the bottom", In *IOP Conference Series: Materials Science and Engineering*, **870**(1), p. 012174 (2020).
29. Doo, J.H., Ha, M.Y., Min, J.K., et al. "An investigation of cross-corrugated heat exchanger primary surfaces for advanced intercooled-cycle aero engines (Part-I: Novel geometry of primary surface)", *International Journal of Heat and Mass Transfer*, **55**(19–20), pp. 5256–5267 (2012).
30. Abbaszadeh, M., Ababaei, A., Arani, A.A.A., et al. "MHD forced convection and entropy generation of CuO-water nanofluid in a microchannel considering slip velocity and temperature jump", *Journal of the Brazilian Society of Mechanical Sciences and Engineering*, **39**(3), pp. 775–790 (2017).
31. Rahman, M.M., Alam, M.S., Al-Salti, N., et al. "Hydromagnetic natural convective heat transfer flow in an isosceles triangular cavity filled with nanofluid using two-component nonhomogeneous model", *International Journal of Thermal Sciences*, **107**, pp. 272–288 (2016).
32. Gibanov, N.S., Sheremet, M.A., Oztop, H.F., et al. "Effect of uniform inclined magnetic field on natural convection and entropy generation in an open cavity having a horizontal porous layer saturated with a ferrofluid", *Numerical Heat Transfer, Part A: Applications*, **72**(6), pp. 479–494 (2017).
33. Pak, B.C., and Cho, Y.I. "Hydrodynamic and heat transfer study of dispersed fluids with submicron metallic oxide particles", *Experimental Heat Transfer an International Journal*, **11**(2), pp. 151–170 (1998).
34. Landauer, R. "The electrical resistance of binary metallic mixtures", *Journal of Applied Physics*, **23**(7) pp. 779–784 (1952).
35. Davis, H.T., Valencourt, L.R., and Johnson, C.E. "Transport processes in composite media", *Journal of the American Ceramic Society*, **58**(9–10), pp. 446–452 (1975).
36. Cui, W., Shen, Z., Yang, J., et al. "Modified prediction model for thermal conductivity of spherical nanoparticle suspensions (nanofluids) by introducing static and dynamic mechanisms", *Industrial & Engineering Chemistry Research*, **53**(46), pp. 18071–18080 (2014).
37. Oztop, H.F. and Abu-Nada, E. "Numerical study of natural convection in partially heated rectangular enclosures filled with nanofluids", *International Journal of Heat and Fluid Flow*, **29**, pp. 1326–1336 (2008).
38. Ali, M.M., Akhter, R., and Alim, M.A. "Magneto-mixed convection in a lid driven partially heated cavity equipped with nanofluid and rotating flat plate", *Alexandria Engineering Journal*, **61**(1), pp. 257–278 (2022).
39. Nasrin, R., Alim, M.A., and Chamkha, A.J. "Buoyancy-driven heat transfer of water-Al₂O₃ nanofluid in a closed chamber: effects of solid volume fraction, Prandtl number and aspect ratio", *International Journal of Heat and Mass Transfer*, **55**(25–26) pp. 7355–65 (2012).
40. Taylor, C. and Hood, P. "A numerical solution of the Navier-Stokes equations using the finite element technique", *Computer and Fluids*, **1**, pp. 73–89 (1973).
41. Dechaumphai, P., *Finite Element Method in Engineering*, 2nd Ed, Chulalongkorn University Press, Bangkok (1999).
42. Zienkiewicz, O.C. and Taylor, R.L., *The Finite Element Method*, Fourth Edition, McGraw-Hill (1991).
43. Gauss, C.F., *A New Method of Integral Values Through the Approximation of Inventing*, Gottingae: Apud Henricum Dietrich (1815).
44. Reddy, J.N., *An Introduction to Finite Element Analysis*, McGraw-Hill, New-York (1993).
45. Zeinkiewicz, O.C., Taylor, R.L., and Too, J.M. "Reduced integration technique in general analysis of plates and shells", *International Journal for Numerical Methods in Engineering*, **3**, pp. 275–290 (1971).
46. Bunch, J.R. and Hopcroft, J.E. "Triangular factorization and inversion by fast matrix multiplication", *Mathematics of Computation*, **28**(125), pp. 231–236 (1974).
47. Ali, M.M., Alim, M.A., Akhter, R., and Ahmed, S.S. "MHD natural convection flow of CuO/water nanofluid in a differentially heated hexagonal enclosure with a tilted square block", *International Journal of Applied and Computational Mathematics*, **3**(1), pp. 1047–1069 (2017).
48. Ali, M.M., Alim, M.A., and Ahmed, S.S. "Oriented magnetic field effect on mixed convective flow of nanofluid in a grooved channel with internal rotating cylindrical heat source", *International Journal of Mechanical Sciences*, **151**, pp. 385–409 (2019).
49. Ali, M.M., Akhter, R., and Alim, M.A. "Hydromagnetic natural convection in a wavy-walled enclosure equipped with hybrid nanofluid and heat generating cylinder", *Alexandria Engineering Journal*, **60**(6), pp. 5245–5264 (2021).

Biographies

Mohammad Mokaddes Ali is a Professor at the Department of Mathematics in Mawlana Bhashani Science and Technology University, Bangladesh. He received his BSc and MSc in Mathematics from Jahangirnagar University, Savar, Bangladesh and PhD

in Fluid Mechanics from the same university. He also received his MPhil in Fluid Mechanics from Bangladesh University of Engineering and Technology, Dhaka, Bangladesh. His research interests include CFD, heat transfer, nanofluids, and biofluids. He has authored/co-authored more than thirty-five research publications.

Sayed Rushd is an Assistant Professor at the Department of Chemical Engineering at King Faisal University. In addition to teaching, he is involved as a principal and co-principal investigator in different research projects. His current research interests include the dynamics of multiphase-flows, water treatment, and desalination. Prior to joining KFU, he was a Research Associate at Texas A&M University at Qatar. Earlier, he worked as a Project Engineer (Matrikon Inc., Calgary, AB, Canada). He holds a PhD degree in Chemical Engineering from the University of Alberta. Dr. Rushd has authored/co-authored more than thirty technical publications.

Rowsanara Akhter is an Assistant Professor at the Department of Electrical and Electronic Engineering at The International University of Scholars, Dhaka,

Bangladesh. She received her BSc and MSc in Mathematics from Jahangirnagar University, Savar, Bangladesh and PhD in Fluid Mechanics from the same university. She also received her MPhil in Fluid Mechanics from Bangladesh University of Engineering and Technology, Dhaka, Bangladesh. Her research interests include CFD, heat transfer, nanofluids, and magneto-hydrodynamics. She has authored/co-authored more than twenty research publications.

Md. Abdul Alim is a Professor at the Department of Mathematics in Bangladesh University of Engineering and Technology, Dhaka, Bangladesh. He received his BSc in Mathematics from University of Dhaka, Bangladesh and MSc in Applied Mathematics from the same university. He also received his MPhil in Fluid Dynamics from Bangladesh University of Engineering and Technology, Dhaka, Bangladesh, and PhD in CFD, Combustion and Heat transfer from Loughborough University, Loughborough, Leicestershire, UK. His current research interests include CFD, combustion, heat transfer, turbulence, and optimization. Dr. Alim has authored/co-authored more than two hundred research publications and reviewed more than three hundred international journals/conference proceedings.